REGENERATION OF BORON-OXYGEN RELATED DEGRADATION IN Cz-Si PERC-TYPE SOLAR CELLS AT HIGH TEMPERATURES

Axel Herguth, Christian Derricks and Giso Hahn
University of Konstanz, Department of Physics, 78457 Konstanz, Germany
Author for correspondence: axel.herguth@uni-konstanz.de

ABSTRACT: Boron-oxygen related light induced degradation (BO-LID) may be eliminated by applying a regeneration process which converts the recombination active 'degraded' defects responsible for BO-LID into an inactive 'regenerated' state. As industrial mass production demands for fast, inline-capable processes and as the regeneration reaction accelerates with increasing temperature, it seems straightforward to increase treatment temperature. However, it is found that a reverse reaction destabilizes the 'regenerated' state at high temperatures and thus the 'regenerated' state is not necessarily the preferred defect state at high temperatures. Within this contribution it is investigated up to which temperature the regeneration process can be applied for boron-doped Cz-Si PERC solar cells. Experiments are accompanied and compared to theoretical predictions. In addition, it is found that the samples under investigation suffer from a second LID effect. Whether this can be attributed to LeTID, degradation of surface passivation quality or a different mechanism remains unclear.
Keywords: Degradation, BO-LID, LeTID, Cz-Si, PERC, Simulation

1 INTRODUCTION

The efficiency potential of p-type PERC (passivated emitter and rear) solar cells surpasses that of full area Al alloyed cells due to its better rear side passivation. As the additional process complexity comes down to higher costs per cell, this advantage only pays off from an economic point of view, if the excess charge carrier lifetime in the bulk τ_b is sufficiently high so that rear side passivation becomes more and more the limiting factor.

However, it is known that rather high qualitative boron-doped monocrystalline Cz-Si suffers from boron-oxygen related light induced degradation (BO-LID) that can, if the worst comes to the worst, push τ_b down into the low two-digit µs region [1] – too low for the PERC advanced rear passivation to pay off.

As of 2006 it is known that BO-LID is curable by a treatment called 'regeneration' consisting of excess carrier injection (often done by illumination) while the sample is kept at an elevated temperature [2,3]. Within the regeneration treatment the harmful defect converts into an inactive 'regenerated' state which is, in contrast to the initial state prior to defect activation, insensitive to illumination under cell/panel working conditions.

Of course, the regeneration treatment can only suit industrial mass production, if it can be applied either in inline mode (time frame of dozens of seconds) or batch mode (time frame of minutes). Both modes require ways to accelerate the regeneration treatment.

It was found that higher temperatures accelerate the regeneration reaction, as well as injection does [2,3]. However, from lifetime studies it was also found that a counter reaction (Redegradation or Destabilization) exists that renders the regenerated defect state more and more instable for temperatures above ~200°C [2,3,4]. Hence, the regeneration treatment at temperatures too high does not result in a majority of defects in the regenerated state. In other words, stabilizing lifetime and thus efficiency via a regeneration treatment does not work anymore.

Within this contribution, regeneration of BO-LID in Cz-Si PERC solar cells in the high temperature regime >200°C is investigated both from a theoretical point of view and in experiments in order to verify the theoretical construct that can be used to predict the impact of the regeneration process even on unknown samples.

2 THE THEORY BEHIND BO-LID (IN PARTS)

The defect responsible for the BO-LID is known to feature at least three different states (see Fig. 1, [2,3]): the recombination inactive 'annealed' state A which is instable under illumination at typical cell/panel working conditions; the recombination active 'degraded' state B; the recombination inactive 'regenerated' state C which is stable under typical cell/panel working conditions. The defect may convert between these states as shown in Fig. 1 where also typical temperature and illumination conditions are summarized under which the respective reactions are known to occur. From experiment it is clear that there exists a reaction path converting the defect from C to A, however, it is hard to decide whether it is a direct reaction connecting C and A or whether it is a two-step reaction C to B to A. In the following this reaction will be treated as redegradation reaction from C to B. State conversion may be described by rate equations of the kind

$$\dot{n}_B = -\left(\kappa_{BA} + \kappa_{BC}\right)\cdot n_B + \kappa_{AB}\cdot n_A + \kappa_{CB}\cdot n_C \qquad (1)$$

where n_j ($\Sigma_j n_j = 1$) is the occupation of the j state in the defect pool and κ_{ij} represent the conversion rates. The whole reaction scheme including especially the complete rate equation system used within this contribution is described in [3] in more detail.

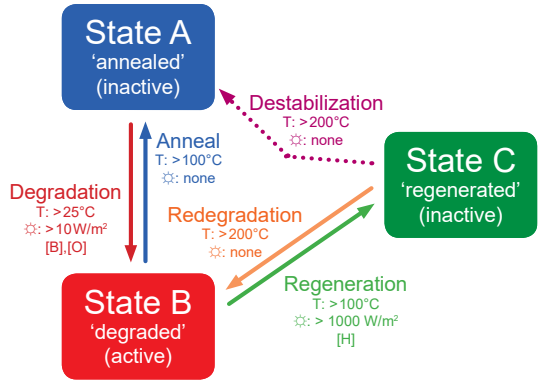

Figure 1: Sketch of the 3-state model of the defect responsible for BO-LID including experimental conditions for which the different reaction paths are active (after [2,3]).

All reactions seem to be describable by an Arrhenius-type temperature dependence (thermally activated) following the formula

$$\kappa_{ij}(T, p_0, \Delta n) = \kappa^*_{ij}(p_0, \Delta n) \cdot \exp\left(-\frac{E_{ij}}{k_B T}\right) \qquad (2)$$

with κ^*_{ij} being the specific pre-exponential factor and E_{ij} the specific activation energy of the respective reactions between state i and j (i,j = A,B,C).

However, one should keep in mind that the kinetic parameters of the different reactions at work were typically not determined in the whole temperature range used in this contribution.

3 THEORETICAL PREDICTIONS

The activation energies of degradation $E_{AB} = 0.475$ eV and anneal $E_{BA} = 1.32$ eV were taken from [5], while those of regeneration $E_{BC} = 1.0$ eV and redegradation $E_{CB} = 1.25$ eV originate from [4]. The pre-exponential factors of anneal $\kappa^*_{BA} = 7.4\times10^{12}$ s^{-1} [5] and redegradation $\kappa^*_{CB} = 5\times10^{9}$ s^{-1} [4] are treated as constant. The factor of degradation was adapted from $\kappa^*_{AB}(p_0 = 1\times10^{16}\,\text{cm}^{-3}) = 4\times10^{3}$ s^{-1} [5] to the doping of the used PERC cells using $\kappa^*_{AB} \sim p_0^2$ [5]. An enhancement of degradation due to injection level as proposed by e.g. Hamer [6] was neglected, as injection level Δn under the experimental conditions applied in this investigation was considered small compared to doping p_0.

The reaction rate of regeneration depends on various parameters like the thermal history (especially the fast firing process) [7], therefore the reaction rate of regeneration was 'calibrated' by an in-situ monitored regeneration treatment at reasonably low temperature [8] yielding $\kappa^*_{CB} = 3\times10^{9}$ s^{-1}.

The resulting reaction rates in dependence of temperature are shown in Fig. 2. As can be seen, anneal rate κ_{BA} and regeneration rate κ_{BC} are almost comparable, but for higher temperatures, anneal rate surpasses regeneration rate. In addition, both rates exceed the rate of degradation κ_{AB} for high temperatures by far.

The colored regions in Fig. 2 show the worst case estimation of uncertainty of the respective rates taking a 1% uncertainty in E_{ij} and κ_{ij} into account in order to provide a feeling for the uncertainty encountered in the simulation. The uncertainty of all above mentioned values in literature exceeds 1% thus meaning that simulation probably depicts correctly the general trend, but fails to deliver exact results.

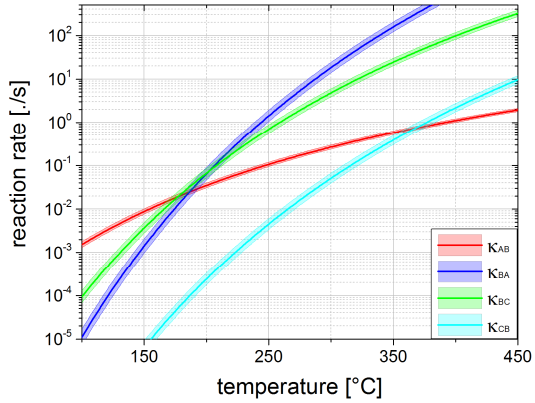

Figure 2: Calculated reaction rates versus temperature. Colored areas depict the uncertainty.

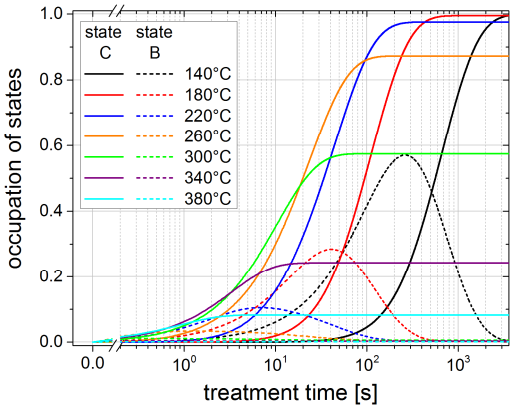

Figure 3: Simulated occupation of states during treatment at different temperatures.

Fig. 3 shows the simulated occupation of states during the treatment at the set temperatures used later on in the experiment. Curves were calculated using the reaction system described above (and in more detail in [3]) implemented in CASSANDRA [9].

Five details should be noted: (I) Long-term equilibrium of state C (solid lines) (and of states A and B as well) is reached faster for increasing temperature. (II) Maximal occupation of state B (dashed lines) occurs faster, but less pronounced with increasing temperature. Above 260°C almost no occupation of state B occurs anymore. (III) Long-term equilibrium value of state C decreases with increasing temperature. As long-term occupation of state B is always negligible, a decreasing occupation of state C implies an increasing occupation of state A. (IV) As both states A and C feature negligible recombination activity, only the occupation of the recombination active state B has an observable influence. Therefore, monitoring the occupation of states during the treatment, gets harder with increasing temperature. (V) Even though the occupation of state A and C may not be distinguished during the treatment, defects in state A and C will react differently when exposed to degradation conditions (low temperature, low intensity illumination): Defects in state A will convert to state B observable as BO-LID while defects in state C will remain stable.

Long-term equilibrium occupation of states versus temperature is depicted in Fig. 4 showing the continuous shift of preference within the defect pool. The colored areas represent the worst case estimation of uncertainty resulting from the uncertainty of rates in Fig. 2.

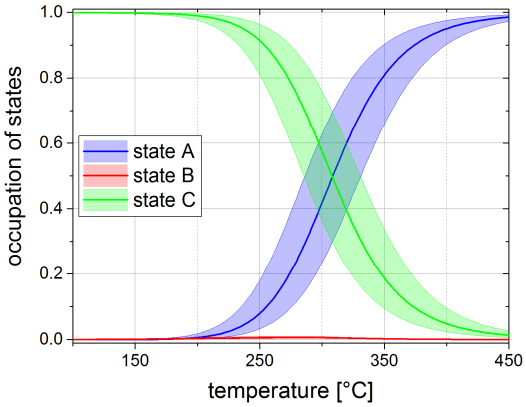

Figure 4: Simulated long-term equilibrium occupation of states versus temperature using the rates shown in Fig. 2. Colored areas depict the uncertainty.

4 EXPERIMENT

4.1 Setup

State-of-the-art boron-doped (~1.2 Ωcm) Cz-Si PERC-type solar cells are used in the experiments. The solar cells were neither annealed, nor degraded prior to the experiments.

Two cells were treated separately: The first was used to quantify the extent of BO-LID by low temperature, low intensity degradation (gray data in Fig. 7). The second was used to obtain the regeneration rate at ~150°C (Fig. 5) used as 'calibration' for the simulation.

The rest of the cells was subjected to illumination on a hotplate in the temperature range of 140 to 380°C. It should be noted that the actual sample temperature may deviate from these set values. Halogen incandescent lamps were used to illuminate the samples with ~2 suns (current equivalent according to [10]).

In order to monitor the progress of the treatment, samples were removed from the hotplate and V_{OC} was measured according to STC.

After the treatment, the cells were exposed to degradation conditions (~35°C, ~0.15 suns, current equivalent according to [10]) to convert defects in state A to state B.

4.2 Preliminary test

As the experiment aims at the long-term equilibrium occupation of states, monitoring the progress might seem irrelevant, however, a first test revealed that monitoring is essential. Fig. 5 shows the evolution of V_{OC} of a cell treated at 150°C and 1 sun intensity.

As expected, V_{OC} drops and recovers due to boron-oxygen related degradation and regeneration in the first 10^4 s (~2.5 h). Then, however, V_{OC} drops and (partly) recovers for a second time – an effect not expectable for BO-LID. It remains unclear, whether this second drop is due to LeTID [11] also occurring in Cz-Si as suggested in [12,13], a degradation of surface passivation quality as shown in [14] or a completely different effect.

In consequence, long-term equilibrium concerning BO-LID is virtually impossible to determine. The best estimation seems to be the maximum value enforced by BO regeneration and the second drop. Unfortunately, this means that the occupation of state C is systematically underestimated giving rise to the asymmetric uncertainty bars in V_{OC} shown in Fig. 8 and that monitoring the progress is mandatory, even if this induces other uncertainties as well.

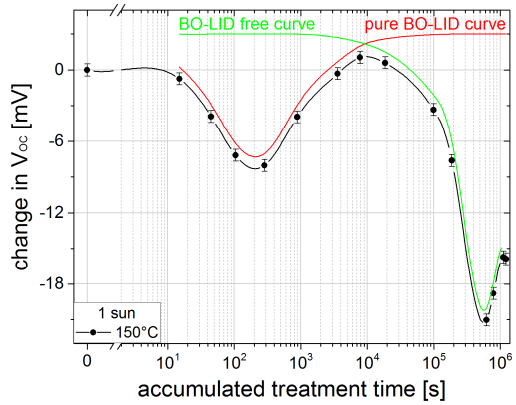

Figure 5: Evolution of V_{OC} during treatment at 150°C and 1 sun illumination intensity. The green and red line depict hypothetical progressions.

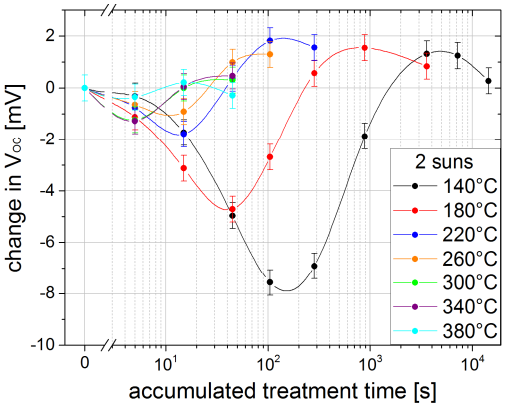

Figure 6: Evolution of V_{OC} during the treatment at various temperatures and 2 suns illumination. Spline lines are only a guide to the eye.

4.3 High temperature treatment

Fig. 6 shows the monitoring results during the treatment at different temperatures. As can be seen, the coldest data set (140°C, black) features the slowest degradation-regeneration-cycle. With rising temperature (180°C, red; 220°C, blue), dynamics are accelerated and the maximal loss decreases, just like simulation has predicted. For even higher temperatures, amplitude decreases further and becomes more and more insignificant, again just like simulation has predicted.

The slight decrease of V_{OC} in the end of every curve shows the beginning of the second drop as depicted in Fig. 5 and marks the point at which treatment was aborted. Nevertheless, a slight loss already occurred.

4.4 Subsequent BO-LID

Fig. 7 shows the results of the subsequent BO-LID treatment at 35°C and 0.15 suns illumination used to convert defects in state A into state B making them distinguishable from defects in state C.

Almost no loss is observable for the lowest treatment temperature (140°C, black) thus meaning almost all defects were -as intended- in state C and not A. Increasing treatment temperature leads to more pronounced losses, indicating a gradual shift of equilibrium from state C to A, again just as simulation has predicted. For even higher temperatures losses would probably converge to the full degradation drop of an untreated sample (gray).

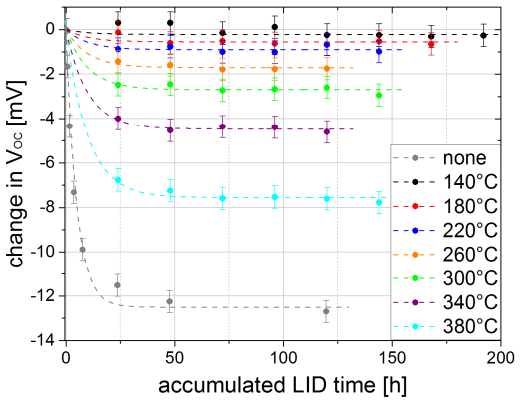

Figure 7: Evolution of V_{OC} during the subsequent BO-LID treatment at ~35°C and 0.15 suns illumination. Dashed lines represent exponential decay curves yielding the long-term drop in V_{OC}.

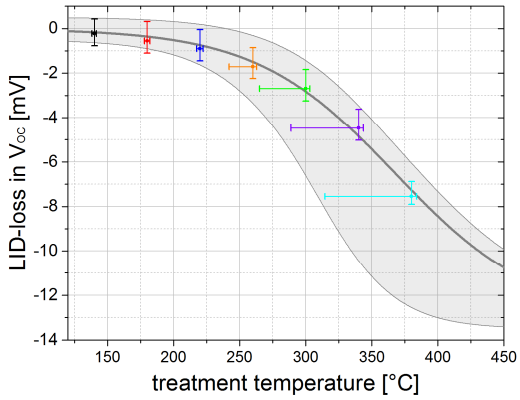

Figure 8: Loss in V_{OC} after BO-LID (Fig. 7) versus treatment temperature. The gray line represents a fit to the data, the gray area takes the experimental uncertainty into account.

4.4 Discussion

The long-term BO-LID loss in V_{OC} from Fig. 7 versus treatment temperature is plotted in Fig. 8. At first glance, Fig. 8 seems to resemble the predicted 'S'-shaped curve in Fig. 4, however, with regard to slope the graphs differ. One could object that Fig. 4 and Fig. 8 do depict substantially different entities and that the 'S'-shape in occupation (Fig. 4) does not necessarily translate to V_{OC} (Fig. 8) without distortion. Therefore, simulation was not only done for the occupation of states but also for the corresponding V_{OC} curve showing that this is not the reason for the discrepancy of Fig. 4 and Fig. 8.

Uncertainty in the input parameters of the simulation, of course, lead to uncertainty in the prediction of occupation as shown in Fig. 4. This may indeed lead to a slight change in slope, but the major effect is a shift on the temperature axis.

The major point of uncertainty is probably found in the experimental data at high temperatures. Firstly, BO related long-term equilibrium was probably not reached as the treatment was broken off too early taking the second LID drop into account. This implies an overestimation of V_{OC} losses and thus introduces a systematic asymmetric uncertainty in V_{OC} loss. Secondly, removing the sample multiple times for monitoring also means that the sample has to heat up again delaying dynamics. Especially for short treatment durations, 'true' temperature is applied shorter than intended and dynamics will have evolved less than expectable from Fig. 3 (calculated with constant temperature). The third point concerns temperature itself. At high temperatures, solar cells tend to bow due to bimetallic stress between the printed Al contact (large coefficient of thermal expansion) and the silicon wafer (small coefficient of thermal expansion). Thus direct thermal contact is hardly present if the sample is not pressed/sucked to the hotplate – which was not the case in the experiment at least for temperatures exceeding 300°C. In consequence, sample temperature may deviate strongly from hotplate temperature and may show lateral inhomogeneity.

The uncertainty in temperature in Fig. 8 was estimated from radiative heat transfer (Stefan-Boltzmann law) resulting in a rather large uncertainty at high temperatures (> 300°C) and comparably low uncertainty at low temperatures (< 300°C). Taking these uncertainties into account, the slopes of Fig. 4 and Fig. 8 match better.

5 CONCLUSIONS

The 3-state model of BO-LID can be successfully used to describe at least the trend at high temperatures for state-of-the-art PERC-type solar cells: Occupation of the regenerated state decreases with increasing temperature above a certain threshold temperature.

However, uncertainty in the input parameters of the simulation yields, of course, uncertainty in prediction complicating exact predictions. In addition, experimental uncertainty in temperature encountered in the presented results hampers a clear assessment of the threshold temperature up to which BO-LID is limited to a certain degree.

Furthermore, it was found that the PERC-type solar cells under investigation suffer from a second LID effect. Whether this can be attributed to LeTID also occurring in Cz-Si, a degradation of surface passivation quality or a completely different effect, remains unclear.

ACKNOWLEDGEMENT

Part of this work was supported by the German Federal Ministry for Economic Affairs and Energy under contract numbers 0325877C and 0324001. The content is the responsibility of the authors.

REFERENCES

[1] K. Bothe, R. Sinton, J. Schmidt, Progress in Photovoltaics **13** (2005) 287
[2] A. Herguth, G. Schubert, M. Kaes, G. Hahn, Proceedings 21st European Photovoltaic Solar Energy Conference (2006), 530
[3] A. Herguth, G. Hahn, Journal of Applied Physics **108** (2010) 114509
[4] S. Wilking, C. Beckh, S. Ebert, A. Herguth, G. Hahn, Solar Energy Materials & Solar Cells **131** (2014) 2
[5] K. Bothe, J. Schmidt, Journal of Applied Physics **99** (2006) 013701
[6] P. Hamer, B. Hallam, M. Abbott, S. Wenham, Physica Status Solidi RRL **9**(5) (2015), 297
[7] S. Wilking, S. Ebert, A. Herguth, G. Hahn, Journal of Applied Physics **114** (2013) 194512
[8] S. Wilking, M. Foster, A. Herguth, G. Hahn, Solar Energy Materials & Solar Cells **142** (2015) 87
[9] A. Herguth, S. Wilking, Energy Procedia **124** (2017) 60
[10] A. Herguth, Energy Procedia **124** (2017) 53
[11] F. Kersten et al., Solar Energy Materials & Solar Cells 142 (2015) 83
[12] F. Fertig et al., Energy Procedia **124** (2017) 338
[13] D. Chen et al., Solar Energy Materials & Solar Cells **172** (2017) 293
[14] D. Sperber, A. Graf, D. Skorka, A. Herguth, G. Hahn, IEEE Journal of Photovoltaics, accepted, doi: 10.1109/JPHOTOV.2017.2755072